Surface features of the lower atmosphere of HD 82558(= LQ Hydrae)

ARTICLE *in* ASTRONOMY AND ASTROPHYSICS · JANUARY 1993

Impact Factor: 4.38

John B. Rice
Brandon University

Jaymie M. Matthews
University of British Columbia - Vancouver

Astron. Astrophys. 268, 671–684 (1993)

ASTRONOMY AND ASTROPHYSICS

Surface features of the lower atmosphere of HD 82558(= LQ Hydrae)

K.G. Strassmeier[1]⋆, J.B. Rice[2]⋆, W.H. Wehlau[3]⋆ ⋆⋆, G.M. Hill[3]⋆⋆, and J.M. Matthews[4] ⋆⋆⋆ †

[1] Institut für Astronomie, Universität Wien, Türkenschanzstraße 17, A-1180 Wien, Austria
[2] Department of Physics, Brandon University, Brandon, Manitoba R7A 6A9, Canada
[3] Department of Astronomy, University of Western Ontario, London, Ontario N6A 3K7, Canada
[4] Département de Physique, Université de Montréal, Montréal H3C 3J7, Canada

Received May 13, accepted November 4, 1992

Abstract. We present simultaneous high-resolution CCD spectra and $UBVRI$ photometry of the very active, young, single K2 dwarf star LQ Hya. The star displays extreme chromospheric activity as well as having a large and variable spot distribution. We applied the Doppler-imaging technique to nine different photospheric absorption lines of various strength. By averaging all individual maps together spurious surface features from one spectral line are suppressed in the final map and only consistent features show up. This greatly enhances the reliability of our Doppler image of LQ Hya. Individual images obtained from the weak line profiles together with the photometry yielded mainly low-latitude surface features. The strongest lines (e.g. Ca I 6439) together with photometry yielded large features at the rotation pole. The surface temperature range is only a few hundred degrees in agreement with simultaneous $UBVRI$ photometry. Four such starspot regions were detected from Doppler imaging. Extended regions of lesser temperature depression are also evident. Additionally we found rotational modulation of certain temperature-sensitive line ratios in agreement with simultaneous near-IR continuum photometry, verifying the "cool" nature of the starspots on LQ Hya.

Chromospheric parameters were computed from Hα as a function of rotational phase. Some line parameters seem to vary in phase with the photospheric line-depth ratios and the photometric light curve. We present evidence that lower electron densities occur at times when a cool starspot is in view, indicating a less dense chromosphere above a spotted region. Variations of the Hα emission-peak asymmetry seem to show extrema when unspotted regions cross the stellar central meridian. Although not conclusive this would be consistent with near-tangential chromospheric velocity fields in the Hα-forming layer probably surrounding photospheric spots.

Key words: starspots – stars: atmospheres of – stars: activity of – stars: HD 82558

1. Introduction

LQ Hya = HD 82558 ($\alpha = 9^h32^m25^s$, δ = -11°11′06″ 2000.0, V = 7.8 mag) is a rapidly rotating, single K2V star probably just arriving on the zero-age main sequence (ZAMS). It is not clear whether the star is already undergoing the rapid loss of angular momentum typical for low-mass stars after arrival on the ZAMS or just experiencing the spinup during the last stage of its pre-main sequence evolution due to contraction towards the ZAMS (cf. Simon 1990).

From its high lithium abundance Fekel et al. (1986a) classified LQ Hya as a young BY Draconis variable "at least as young as the youngest Pleiades star", while Vilhu et al. (1991) even suggest that it is a pre-main sequence object. The galactic velocity components for LQ Hya, although uncertain due to a poorly determined parallax, are also consistent with it being a young disk star. As would be expected from its Li age, the star shows very strong chromospheric Ca II H and K emission-line surface fluxes of 10^{6-7} erg cm^{-2}s^{-1} (Strassmeier et al. 1990), reminiscent of a number of rapidly-rotating K dwarfs in the Pleiades cluster found by van Leeuwen & Alphenaar (1982). From an evolutionary viewpoint, this group of stars is rotating much too rapidly, indicating that almost no braking had occurred.

Send offprint requests to: K.G. Strassmeier

⋆ Visiting astronomer: Canada-France-Hawaii Telescope, operated by the National Research Council of Canada, the Centre National de la Recherche Scientifique de France and the University of Hawaii

⋆⋆ Guest observer: Mauna Kea Observatory of the Institute for Astronomy, University of Hawaii

⋆⋆⋆ Visiting astronomer: Cerro Tololo Inter-American Observatory, National Optical Astronomy Observatories, operated by the Association of Universities for Research in Astronomy, Inc., under contract with the National Science Foundation

† Guest observer, University of Toronto Southern Observatory, Las Campanas, Chile

Detailed information about such young stars is relatively rare. The single, post-T Tau star AB Doradus (K0, $v \sin i \approx 80$ km s^{-1}, e.g. Collier-Cameron & Robinson 1989) is probably the most active young star identified so far. Another young star, the primary component of the spectroscopic binary HD 155555 ($\approx$G5-8, $v \sin i$ = 37 km s^{-1}, Pasquini et al. 1991) is another likely candidate. Doppler maps of both stars by Kürster et al. (1992) showed middle and high-latitude spots reaching as high as the visible pole on AB Dor, and a large polar spot on HD 155555. In this paper we add LQ Hya to the list of young stars for which there is disk-resolved information (see also Saar et al. 1992).

LQ Hya is also photospherically active. Broad-band photometry showed V amplitudes of $\approx$0.1 mag with a period of 1.6 days (Strassmeier & Hall 1988). This is in agreement with the observed line broadening of 25 km s^{-1} (Fekel et al. 1986b) and suggests that the photometric variability is due to rotational modulation, presumably by cool starspots. Recently, Jetsu (1990) reported short-term variations of the shape of LQ Hya's light curve on the order of weeks, indicating rapidly changing spot coverage. Ambruster & Fekel (1990) detected a strong ultraviolet flare in four continuum bands between 1250 and 1850 Å, while no enhancement was evident in any of the chromospheric lines.

Within the past few years, much effort has been spent on the development of stellar imaging techniques from high-resolution spectral line profiles (often called "Doppler imaging"). This is a technique to derive a resolved "image" of a star by using the relation between wavelength position across a spectral line and spatial position across the stellar disk. Cool spots on the surface of late-type stars produce periodic distortions in the line profiles which can be followed throughout a rotational cycle. With this technique one routinely achieves resolutions of $\approx$ 10° on the stellar surface.

In this paper we will concentrate on photospheric and chromospheric inhomogeneities on LQ Hya observable at optical wavelengths and present a combined Doppler image made from variations of nine spectral lines and three continuum regions. Section 2 describes our observations. The analysis of our $UBVRI$ light curves with a standard spot modeling computer program is the subject of Sect. 3. Section 4 presents our Doppler-imaging results. In Sect. 5 we determine the chromospheric structure from Hα line-profile variations and absolute Ca II emission-line fluxes. An additional determination of the spot temperature from variations of certain line-depth ratios is presented in Sect. 6. Finally, Sect. 7 summarizes our main conclusions.

2. Observations and data reductions

2.1. Spectroscopy

The spectroscopic observations were made at the Canada-France-Hawaii telescope (CFHT) during the period Jan 29 - Feb 1, 1991. The f/7.4 coudé spectrograph was used in first order with the 1800 g mm^{-1} holographic grating at a resolution of about 82,000. All observations utilized a 2048×2048 pixel CCD resulting in a scale of 0.03 Å/pixel and a useful wavelength range of 60 Å. All integrations on LQ Hya have typical signal-to-noise ratios of 300:1 and were made primarily in three wavelength regions centered at λ6160, 6440, and 6560 Å. The 6160 Å region contains up to nine unblended lines of various strength suitable for Doppler imaging as well as several temperature sensitive line ratios. The 6430 Å region is the one which contains the classical Doppler-imaging lines Fe I at 6430 Å and Ca I at 6439 Å as well as another, fairly unblended, iron line at 6411 Å. The 6560 Å region not only contains Hα but another, moderately strong, unblended iron line suitable for Doppler imaging (Fe I 6546 Å). The 8480 Å region was chosen for a one-time integration because it contains one of the calcium infrared lines and an unblended Fe I line very sensitive to magnetic fields (Fe I 8468, $\lambda g_{\rm eff}/1000$=21.17; Gray 1988). Table 1 is a short summary of measured equivalent widths but also contains some atomic data of the spectral lines used in the analysis. Entries having a $\log gf$ value are the lines used for Doppler imaging. Typical spectra of these wavelength regions are presented in Fig. 1 along with the K1V temperature standard o^2 Eri (Bell & Gustafsson 1989). All spectra were obtained through the standard process of subtracting averaged biases and dividing by image-slicer flat fields taken immediately before or after a stellar integration. To remove the (very small) flat field degradations introduced by the image slicer we have obtained nightly flat field images through a regular slit and divided all stellar and comparison-lamp images by them.

Table 1. Photospheric-line equivalent widths

Line	$\log gf$	χ (eV)	W_λ (mÅ) LQ Hya K2	12 Oph K2	o^2 Eri K1
Fe I 6141.73	-0.50	3.60	187	144	104
Fe I 6151.62	-3.52	2.18	72	72	60
Fe I 6157.73	-1.35	4.07	87	79	61
Fe I 6165.36	...	4.14	60	57	42
Ca I 6166.44	...	2.52	116	102	92
Fe I 6173.34	-3.09	2.22	105	97	76
Ni I 6175.37	...	4.09	56	...	44
Fe I 6180.21	-2.99	2.73	92	...	61
Fe I 6411.66	-0.10	3.65	236	174	141
Fe I 6430.85	-1.85	2.18	187	151	125
Ca I 6439.08	+0.40	2.52	326	220	200
Fe I 6546.24	-1.90	2.76	167	132	113
Fe I 8468.42	...	2.22	244	165	...

Seeing was mostly better than 1″ and integrations were set to 2400 sec or 3200 sec ($\simeq$ 2 % of the rotation period) depending upon air mass. This allowed for a series of nine spectra in each of the three wavelength regions shown in Fig. 1 and covered the rotational phases between 0.09 and 0.67. Unfortunately, a full night was lost to high wind speeds and almost half a night to mechanical problems.

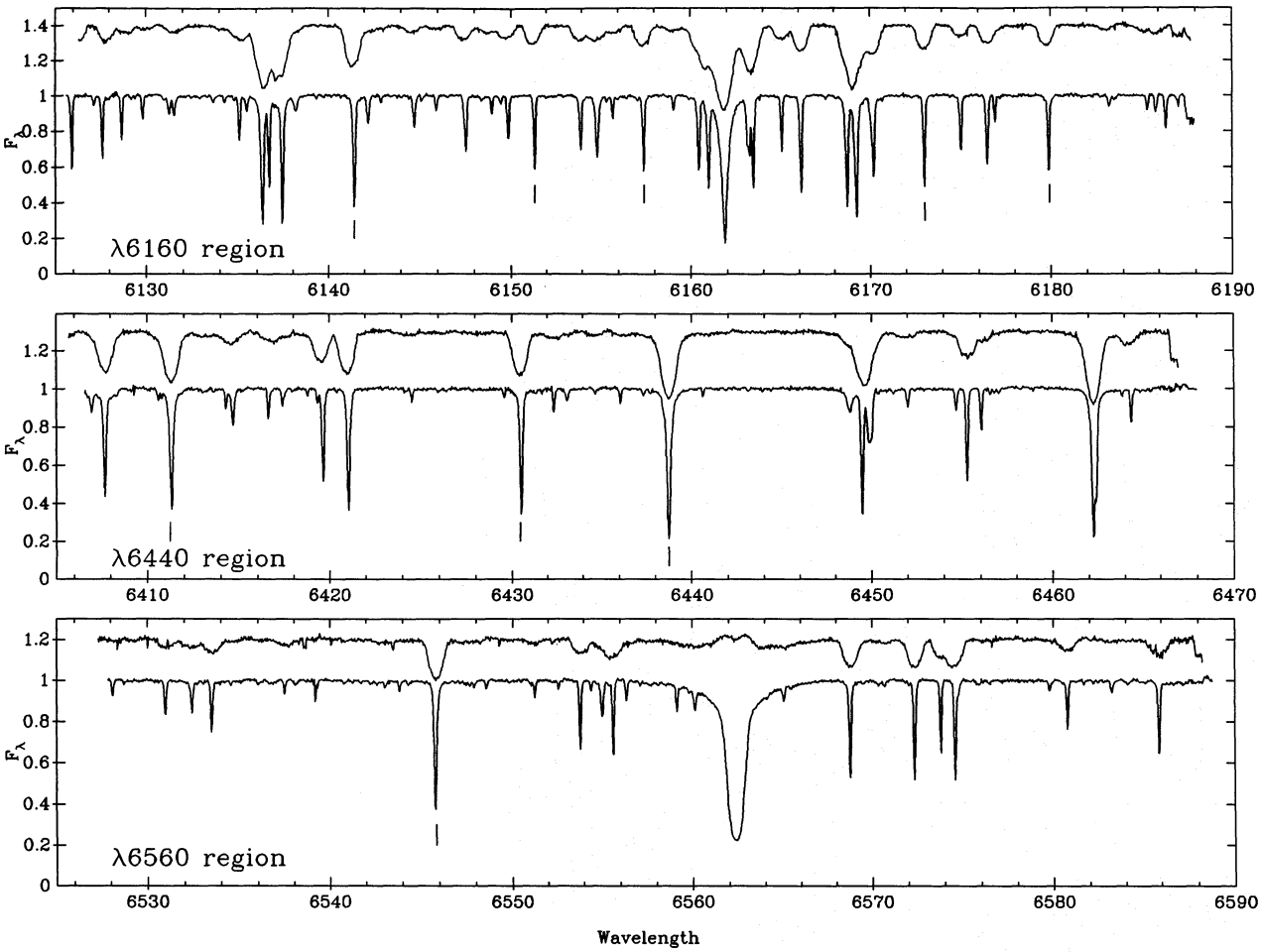

Fig. 1. Typical examples of spectra used in the analysis. In each panel the upper spectrum is LQ Hya and the lower the K1V standard star o^2 Eri. Shown is the full range for three different wavelength regions centered at, from top to bottom, 6160, 6440, and 6560 Å. Resolution is 82 000 or approximately 0.08 Å, S/N is estimated to be around 300:1. The spectral lines used for "Doppler imaging" are marked

2.2. Photometry

The photometric observations were made simultaneously and contemporaneously to the spectroscopic observations with the 0.6-m University of Hawaii telescope on Mauna Kea, the 0.6-m University of Toronto telescope at Las Campanas Observatory, Chile and with the 0.6-m Lowell telescope at Cerro Tololo Interamerican Observatory (CTIO) between Jan 13 and Feb 12, 1991. All observations were made differentially with respect to HD 82477 as the comparison star and HD 82508 as the check star and utilized Johnson UBV and Cousins RI filters. The average nightly standard errors varied from site to site and bandpass to bandpass. The Hawaii and CTIO data show comparable scatter in the UBV bandpasses, but the Hawaii RI measurements have much smaller standard errors than the data from the Chilean sites. Standard errors of approximately 20 mmag were encountered in the U band due to the significantly lower photon count level. The individual $UBV(RI)_C$ observations are available from the IAU Commission 27 "Archive for Unpublished Observations of Variable Stars" as file 242E.

From the average magnitude differences between comparison and check star, and from the mean color indices for the check star (HD 82508) taken from Cutispoto (1991), Fekel et al. (1986a), and Jetsu (1990), we obtain absolute magnitudes and colors for LQ Hya at light-curve maximum (least spottedness) of V=7.774±0.010 ,$U-B$=0.59±0.012, $B-V$=0.865±0.010, $(V-R)_C$=0.51±0.010, and $(V-I)_C$=0.99±0.010 mag. The observed peak-to-peak amplitudes of around 0.1 mag in V and 0.05 in $V-I$ severely affect the "true" color indices. "Maximum" indices are thus less affected by the presence of starspots and thus more representative of the spectral type. These colors agree well with the previously assigned K2V classification (Fekel et al. 1986a).

We separated our photometry into three data sets, one simultaneous to the spectroscopic observations, and the other two prior and after them. The corresponding light and colour curves are presented in Figs. 2a-c. All observations presented in this paper were phased with our new ephemeris of

$$HJD = 2448270.0 + 1.606 \times E, \quad (1)$$

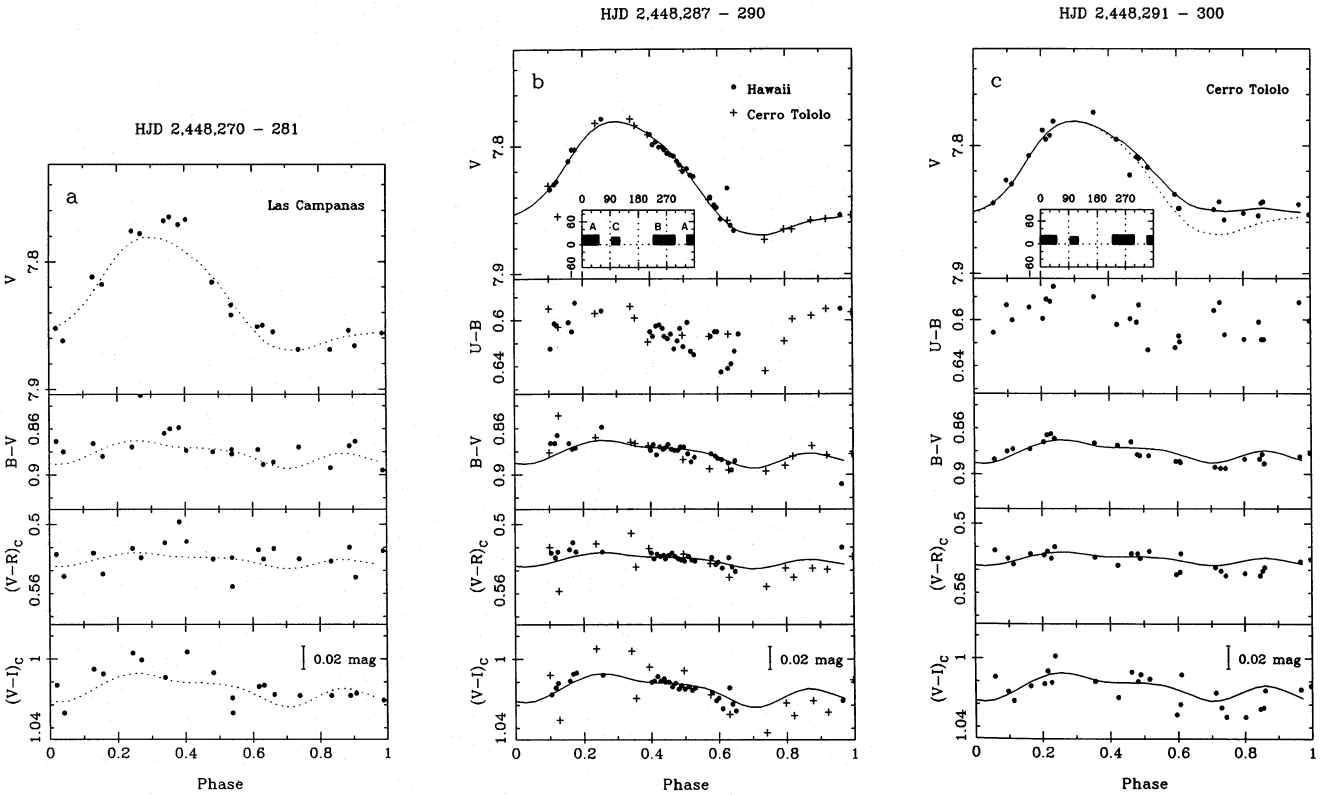

Fig. 2. Differential light and color curves of LQ Hya and the fits with a three-spot model (full lines in panel (*b*) and (*c*)). The three panels represent the data sets mentioned in the text with (*a*) being prior to, (*b*) simultaneous and, (*c*) after the spectroscopic observations. The dotted lines in panels (*a*) and (*c*) are the fits from data set (*b*) repeated for comparison purpose. The inserts in the upper panels are mercator maps of the obtained spot distributions from the spot modeling analysis. No acceptable fit was possible for data set (*a*) due to the steep decline of the light curve at phase 0.5. It is possible that the shape and amplitude of the light curve has changed substantially. Note that all three data sets were obtained within one month

where the initial epoch is arbitrary and the period is the best photometric period from a least-squares fit to our entire data set. We adopt this as the rotation period of LQ Hya (see Sect. 3.2).

3. Light curves and photometric analysis

3.1. Photometric history of LQ Hya

Figure 3 summarizes the existing body of V-band photometry of LQ Hya from the discovery of its light variability in late 1982 (Fekel et al. 1986a) through our most recent data from 1991. Our $UBV(RI)_{\rm C}$ photometry covered only about 20 stellar rotations. Even within this short interval we observed smoothly changing V light amplitudes from 0.103±0.010 mag at the beginning of the observations to 0.067±0.007 mag at the end. (The cited errors are the uncertainties from standard Fourier fits.) The color variations appear to be correlated with the V light curve in that the star is redder at times of light minimum. Cutispoto (1991) pointed out that his 1987 $U-B$ and $B-V$ colors varied in antiphase with the V light curve and suspected the possibility of micro flaring. We do not observe this in our photometry, as seen in Figs. 2a,b,c. Nevertheless, the general behaviour is typical of starspot activity known in RS CVn-type stars (Hall 1991) and suggests a similar cause for LQ Hya. A previous claim by Fekel et al. (1986a) that the starspot distribution on LQ Hya remained stable for 500 days (over 300 rotations) – hence resembling several rapidly rotating Pleiades K dwarfs with extremely stable light curves – cannot be verified from our data. However we point out that the average spot longitudes remained about the same during our one-month span of observations. At the same time, we did observe short-term changes of the light curve *shape* with a typical time scale of few rotation cycles, consistent with changes in spot area. This also agrees with the conclusion of Jetsu (1990) from data in 1989/90 and earlier photometry by Strassmeier & Hall (1988) from 1984/85.

3.2. Rotation and radius of LQ Hya

Photometric periods of spotted stars are known to be intrinsically variable. One possible reason for this is that spots may occur at different stellar latitudes and, with the assumption of solar-like differential rotation, can account for observed period changes of up to 20 % (Strassmeier & Bopp 1992). A particular photometric period could thus be interpreted as the rotation period of the photosphere at the spot's latitude.

Table 2. Photometric spot modeling fits

Data set HJD 2,448+	spot	ΔT (K)	ℓ_1 (°)	ℓ_2 (°)	θ_1 (°)	θ_2 (°)	area (%)
287-290	A	500	337	53	0	25	4.46
	B	500	230	297	0	23	3.64
	C	500	95	120	0	18	1.07
	sum						9.17
291-300	A	500	340	50	0	22	3.64
	B	500	230	297	0	23	3.64
	C	500	95	120	0	18	1.07
	sum						8.35

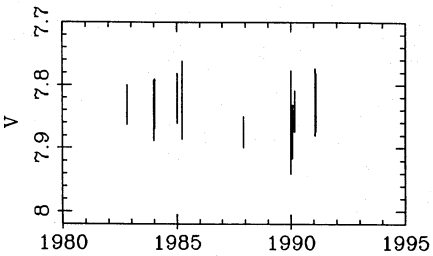

Fig. 3. Long-term light curve behaviour of LQ Hya. The vertical bars indicate the light curves' peak-to-peak amplitudes. Data were taken from Fekel et al. (1986a), Eggen (1984), Cutispoto (1991), Jetsu (1990), and supplemented with our new data from 1991. The star appeared brightest in 1985 with V = 7.764 mag, which we assumed to be the unspotted magnitude, and faintest in 1990 with V = 7.94 mag. Obviously, the full range of amplitudes can vary by up to a factor three, e.g. between late 1987 and early 1990, but there is no clear indication of a cyclic behavior

The absence of an accurate "timekeeper" in a single star like LQ Hya, e.g., the orbital period, forces one to use the "best"-fit photometric period to phase the data. Several period-finding programs were applied and we found the greatest reduction of the sum of the squared residuals at a period of 1.6062±0.0012 days, comparable to the period of 1.598±0.002 days in 1984/85 (Strassmeier & Hall 1988) but significantly shorter than the 1.66-day period in late 1982 through early 1984 from Fekel et al. (1986a). By comparison, we have analyzed Cutispoto's (1991) ESO data from 1987 and found a period of 1.609±0.002 days in good agreement with the period from 1991. From roughly 1984 to 1991, the observed periods are consistent with each other; only the 1982-84 observations indicate a significantly longer period. If LQ Hya undergoes solar-type differential rotation and latitude drift, rotation periods should appear to become progressively shorter at the end of a spot cycle. So far, the available photometry covers too short a baseline in time to justify a more thorough discussion.

With our new value for the equatorial rotational velocity of 24±1.0 km s^{-1} from the line with the smallest FWHM, and with the "best" rotation period of 1.606±0.001 days, the minimum radius of LQ Hya is determined from $R \sin i = P_{\rm rot}\, v \sin i$ to be 0.76±0.03 R$_\odot$. Several sources quote a typical radius of 0.80 R$_\odot$ for a K2 dwarf (e.g. Schmidt-Kaler 1982; Andersen 1991). If we assume this radius for LQ Hya the inclination of the rotation axis may be estimated to be $\approx$ 70±10°, which we adopted throughout this paper.

3.3. Spot modeling

We have applied a modified version of the computer program described originally by Strassmeier (1988) which is based on numerical disk integrations with rectangular spots. Because of the relatively high inclination of $\approx$ 70° we assumed the lower latitude boundary for each spot to be at the stellar equator. The relative spot temperature ΔT (i.e. the temperature difference in the sense, photosphere minus spot) is mainly constrained by the amplitude and shape of the $V-I$ color curve but also by $B-V$ and $V-R$. Any spot-modeling procedure must assume the unspotted brightness of the star which controls the total spotted area and spot temperature in that it scales the theoretical fits to the light and color curves. From the collection of photometry in Fig. 3 we obtain a peak magnitude of V = 7.764 mag in early 1985 and adopt this as the "unspotted" magnitude. If the peak magnitude in 1985 is about as bright as the star has ever been, our light-curve fits should be realistic. In fact, models with unspotted magnitudes brighter by only 0.03−0.04 mag would require additional dimming and reddening by, e.g. a polar spot or a homogeneous background spottedness. Given the K2V spectral classification we adopt an effective surface temperature of 5100 K from the calibration of Bell & Gustafsson (1989). Linear limb-darkening coefficients were taken from the 5000 K, log g=4.0 models of Al-Naimiy (1978).

The model fits to the light curves are also plotted in Fig. 2. Note that the Hawaii photometry was given higher weight in these fits, due to the lower scatter in the $V-I$ and $V-R$ data. Table 2 contains the resulting spot-model parameters for the best fits to two of our three data sets where ℓ is the spot longitude, θ the spot latitude, and "area" the spot area in percent of the entire stellar surface. It is possible that the shape and amplitude of the first data set has changed during the interval of observation and no spot model fit was obtained. The resulting spot temperature for LQ Hya is surprisingly low, ΔT = 500 ± 200 K, relative to previous determinations for most other spotted stars. Nevertheless, the result is relatively robust and fairly insensitive to the choice of unspotted magnitude. By comparison, Saar & Neff (1991) used spectra of the TiO absorption bands to estimate the temperature and projected area of cool spots on LQ Hya and obtained preliminary values of $\Delta T \leq$ 1200 K and $\geq$ 0.22, respectively. While consistent with our determination of $\Delta T_{\rm spot}$ = 500 K, clearly their upper limit of 1200 K is much higher than our value.

4. Multiline Doppler imaging

4.1. Line profile inversion with maximum entropy or Tikhonov error function

Doppler imaging amounts to solving the so called inverse problem. The inverse problem, for stars like LQ Hya that have spots

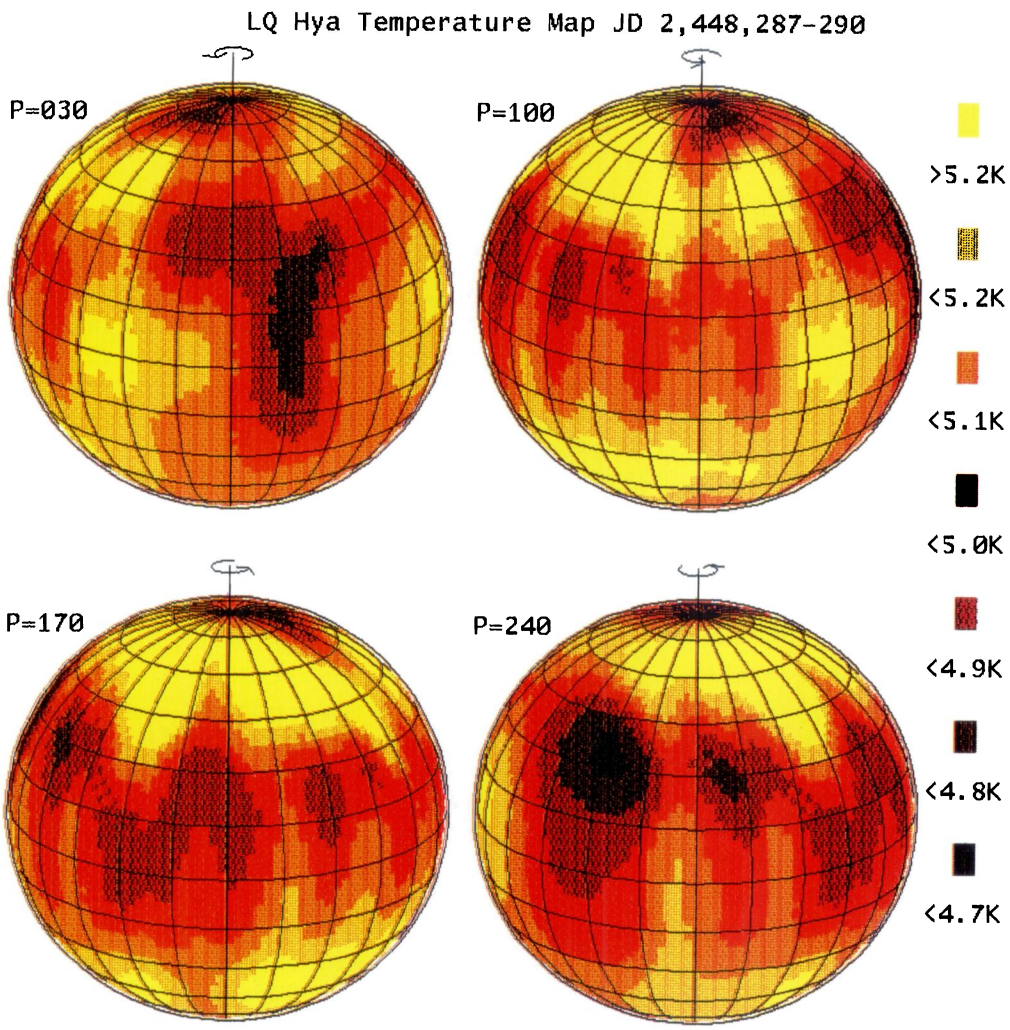

Fig. 4. Combined Doppler image of LQ Hya from 18 maps of 9 lines. The individual images were averaged with equal weights. All reconstructions were performed using simultaneous V, R, and I photometry

of cooler or greater temperature on their surface, amounts to recovering the surface temperature distribution from the integral equation that relates the distribution of surface temperature to the observed line profile and light curve variations. For the maps in this paper local line profiles were computed from a numerical solution of the equation of transfer with the $T_{\rm eff}$ = 4000, 4500, 5000 K, and log g = 2.7 model atmospheres of Kurucz (1979). The model atmospheres are calculated assuming LTE and the local profiles for each small element of the star are obtained from the grid of profiles by interpolation to match the local effective temperature. The basic outline of the computer code used here is given by Rice et al. (1989) and also discussed in Piskunov & Rice (1992). The effects of noise in the data are controlled by a penalty function, or regularizing functional, that prevents the "overinterpretation" of information contained in the line profiles and light curve. The Doppler-imaging code of Rice incorporates a choice between using a maximum entropy penalty function in solving the inverse problem, or using a Tikhonov penalty function. In practice, the choice between these has little significance because normally only small weighting is given to the penalty function where the noise problem is not serious. For the solutions discussed here, only a small weight of Tikhonov penalty function was used for the images. Continuum light variations are also employed by the mapping routine to further constrain our solution.

There are a number of factors which contribute to systematic differences in the maps we obtain for different lines. One is the problem of having the value of the log gf correct. Generally, in temperature sensitive lines, the mapping program compensates for small errors in log gf by adjusting the average temperature of the surface so that the equivalent width of the computed line matches the equivalent width of the observed line. If the log gf is in error by more than about 0.3 or so the problem is usually quite obvious but smaller errors will have small effects that cannot be characterized as a general numerical conclusion. A second systematic difference arises in the strong lines because of the assumption of LTE in calculating local line profiles. One should expect that the core representation in the local line profiles would

be poor for very strong lines. In some cases there may even be core emission present in the actual local line profiles in variable amounts over the stellar surface and we are unable to allow for that. In a star such as LQ Hya, where the $v \sin i$ is relatively small, the errors in representing the local line profiles become serious, especially in the strongest lines where we not only might expect the greatest error in the calculation of the local line profile but where, in addition, the ratio of rotational broadening to local line width is smallest. A third systematic effect is the effect of setting the continuum accurately during data reduction. Errors in judging the correct location of the continuum affect weak lines more than strong lines and would (if the error tends to be systematic) have an effect on the average surface temperature calculated by the program.

4.2. Mapping the photosphere of LQ Hya

We present in Fig. 4 a combined surface map of LQ Hya which is the average of 18 maps made from the data for 9 lines with equal weights. Several useful lines are indicated in the spectra shown in Fig. 1 and those actually used for the line profile inversion are listed with a $\log gf$ value in Table 1. The geometric factors adopted for all maps were $i = 70°$, $v_{\rm eq} = 29.5$ km s^{-1} ($v \sin i = 27.7$ km s^{-1}) with $v_{\rm macro} = 1.5$ km s^{-1} and $v_{\rm micro} = 2.0$ km s^{-1}. The value of $v \sin i$ was chosen on the basis of results from three lines (Ca I 6439, Fe I 6141, and Fe I 6151). The best fit, i.e. the minimum error in fitting the line profiles, was for inclinations near 60° to 70° and for equatorial velocities ($v_{\rm eq}$) between 29.5 to about 31.0 km s^{-1}.

We made two maps for each line using photometry of two passbands per run, in one run the V and I photometry and in a separate run, the V and R photometry. The light curve fit from the Ca I 6439 Å map is shown in Fig. 5a. The fit to the colors $V-I$ and $V-R$ seems poor at first glance but the fit is almost completely within the error bounds of the available data. Note that the fit to phases between 240° and 30° are only weakly governed by the spectroscopy due to its incomplete phase coverage and are more sensitive to the photometry. Typical line profile fits are shown in Fig. 5b.

Figure 6 shows the individual maps for five lines of different strengths with equivalent widths ranging from 326 mÅ for Ca I 6439 to 87 mÅ for Fe I 6157 Å. Their $\log gf$ values range from +0.40 through −3.09, and excitation potentials from 2.22 through 4.08 eV. Only maps using V and I photometry are shown. The individual maps for each line make it fairly clear that the features that show up in the average map are the persistent features in the individual maps. This ensures that spurious features from a single line, caused by noise or systematic errors of some kind in the profile, will be suppressed in the final average map. The best lines for mapping in terms of surface resolution are the weaker lines with narrower local profiles, but these weak lines suffer from more noise problems. By using several weak lines for the average map, we gain the advantage of higher resolution while suppressing the noise factor. However, in doing so we neglect any variations of the size and location of the starspots with height in the photosphere of LQ Hya. Another finding from our multiline approach is that the stronger lines (Ca I 6439, Fe I 6141) tend to be slightly more flat bottomed than the weaker lines and are thus best fitted with a polar or circumpolar spot. This could be due to a physical increase of the spot size with height in the stellar atmosphere but also due to chromospheric "filling in" of the cores of the strong lines and errors in the local line profile because of the lack of knowledge of the proper physical conditions at small optical depths in the atmosphere. We believe that, with the present S/N ratio (especially for the weak lines), we can not reliably discern between such effects.

Two major spot regions are visible at longitudes $\ell \approx 0°$ and $\ell \approx 270°$ and latitudes θ between −20° and +45°. Their temperature contrast is no greater than 500 K, in agreement with the purely photometric results from the previous section. Lower contrast features with $\Delta T \approx 400$ K are also present, one at $\ell \approx 230°$ and $\theta \approx +30°$, and one at or very near the rotation pole with $\ell \approx 70°$ and between 70° and 90° latitude. Our map of LQ Hya is clearly not *dominated* by a polar "cap", as found in Doppler images of other spotted stars, e.g. V711 Tau = HR 1099 (Vogt 1988; Donati et al. 1992), HD 199178 (Vogt 1988), UX Ari (Vogt & Hatzes 1991), EI Eri (Strassmeier et al. 1991), HD 155555 and HD 32918 (Kürster et al. 1992). Curiously, an earlier image of HD 32918 by Piskunov et al. (1990) did not show this polar feature. Two of the EI Eri maps obtained by Piskunov in Strassmeier et al. (1991) also did not reveal a polar cap.

5. Chromospheric structure of LQ Hya

5.1. Ca II emission

Very strong Ca II H and K emission lines well above the nearby stellar continuum indicate the presence of an active chromosphere on LQ Hya. Strassmeier et al. (1990) measured absolute emission line surface fluxes for both lines as well as Hϵ and found values of as large as 10^7 and several 10^6 erg cm^{-2} s^{-1}, respectively. However, their fluxes were based on an empirical $V-R$ color from the old dK0 classification of Bidelman (1981) and must be reduced by ≈ 50 % since the star is most likely a K2V. The revised absolute emission-line surface fluxes based on our measured $V-R$ color and corrected for photospheric contribution are: $\log \mathscr{F}'(H/K) = (6.60/6.77)$ erg cm^{-2} s^{-1} and $\log \mathscr{F}'(H\epsilon) = 6.40$ erg cm^{-2} s^{-1}, typical for what is seen from RS CVn-type binaries.

One high-resolution spectral profile of the λ 8498 Å line of the Ca II infrared triplet was obtained at phase 0.533 (Fig. 7) with the CFHT set-up described in Sect. 2a. This line is the least opaque of the three infrared triplet lines and shows higher emission in strong solar plages and central reversals even in weaker solar plages (Shine & Linsky 1972). For LQ Hya the line core is clearly in emission. To compare its strength with other stars from the extensive data base of Dempsey et al. (1992) we determined fluxes following the procedure described by Linsky et al. (1979). The equivalent width under the line core in a 2-Å bandpass is $W_\lambda = 1.678$ Å and is multiplied with the surface flux

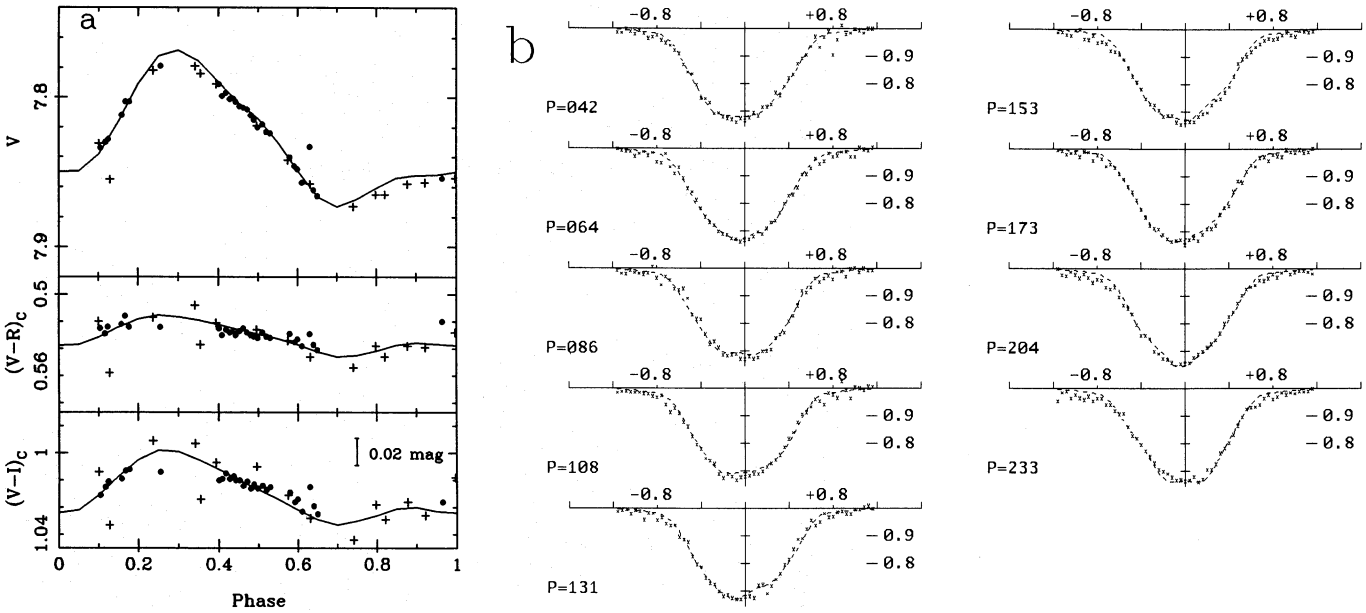

Fig. 5. (*a*) Observed and computed light curves. The line is the fit from the Ca I 6439 Å Doppler map shown in Fig. 6. (*b*) Observed and computed line profiles for Ca I 6439. The line is the computed profile and the points are the observations

at the nearby continuum using our measured $V - I$ color. This yields a surface flux of 3.9 10^6 erg cm^{-2} s^{-1}, almost identical to the flux for V711 Tau = HR 1099 (K1IV), one of the most active RS CVn binaries.

To compare LQ Hya with typical solar plage line profiles, e.g. from the work of Shine & Linsky (1972), we measured core residual intensities at the emission "shoulders" (X_{2V} = 0.865, X_{2R} = 0.880) and at the central reversal (X_3 = 0.855) and find them significantly higher than in solar plages despite that the values for LQ Hya are disk averaged intensities. We note that the photospheric background spectra are different for a G2 and K2 star and that the continuum flux is significantly lower on a K2 star. However, a more relevant comparison is possible when we subtract the photospheric contribution from the LQ Hya scan. The equivalent width of the residual emission, as determined from subtraction of a spectrum of the K2V star 12 Oph (Fig. 7), is 270±15 mÅ. This is also much higher than the corresponding solar-plage value. The ratio of the emission peaks (X_{2R}/X_{2V}) for Ca II 8498 in LQ Hya and in a strong solar plage is 1.017±0.002 and 0.986−1.003, respectively, thus much more asymmetric in LQ Hya than in solar plages. The corresponding parameter for the Hα core emission is 0.977 at phase 0.503, i.e. for Hα the "blue" emission peak is stronger than the "red" peak opposite to Ca II 8498 (compare Fig. 7 with Fig. 8) which is puzzling since it is believed that the Ca infrared triplet lines are also formed in the lower chromosphere and the two spectra were taken on the same night one after the other. We have no ready explanation for this.

5.2. *Balmer Hα emission-line morphology*

Hα emission-line profiles of LQ Hya are shown in Fig. 8 along with a spectrum of o^2 Eri, a K1V standard star. All spectra were recorded simultaneously with the photospheric-line observations (see Sect. 2.1). Like the other spectra, only one half of a rotation cycle was covered. The core of the line is clearly seen in emission with a central reversal at the rest wavelength and the line wings in absorption similar to o^2 Eri. In almost all spectra the "blue" peak of the emission is stronger than the other. Phenomenologically, this is reminiscent of some single dMe stars, e.g. DK Leo, V1005 Ori, and AU Mic in the study of Pettersen (1989). There could be several reasons for this Hα-line asymmetry. First, a weak chromospheric velocity field could shift the peaks relative to the emission line center and the peaks would just appear to have different strengths. Second, the line profile shape of the residual emission could be modulated by bright plages moving across the stellar disk. Third, circumstellar clouds embedded in a hot extended corona might produce transient absorption and/or emission features which, if temporally unresolved, would result in an asymmetric profile. The latter two possibilities require that sometimes during a rotation cycle the "red" peak of the emission appears stronger than the "blue" and this is not what we see. So the effect on the Hα line must be more subtle and is presumably due to a combination of stellar plages moving in and out of view and global and possibly also local velocity fields with enhanced contrast (as for the G8 dwarf ξ Boo A; Toner & Gray 1988). Figure 9 and Table 3 summarize the results of our analysis, which are discussed in detail below.

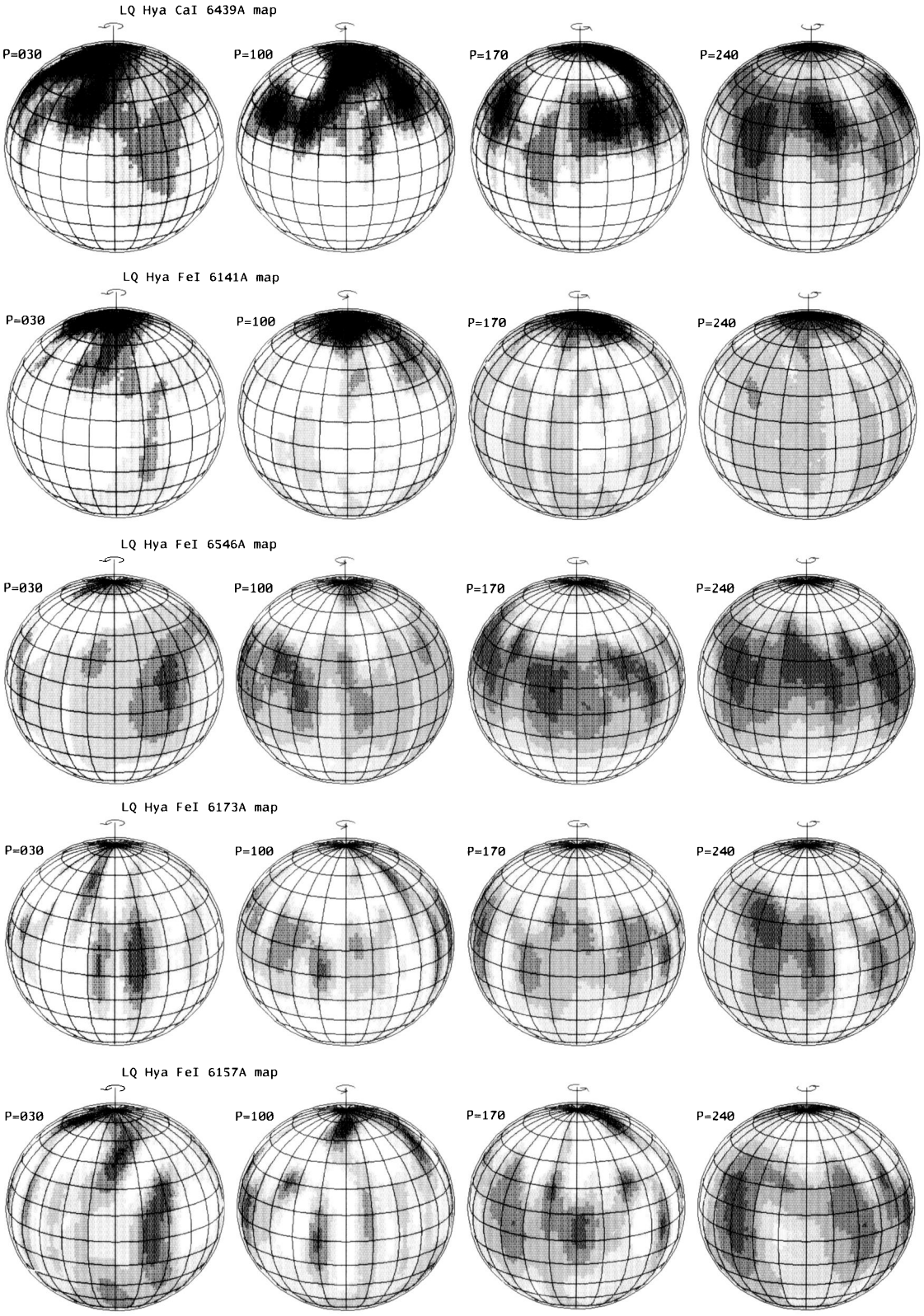

Fig. 6. Individual maps for five lines of different strength. Maps are shown for four phase angles, 30°, 100°, 170°, and 240°, from left to right, respectively. From top to bottom, lines with decreasing equivalent width are shown, Ca I 6439 (W_λ = 326 mÅ), Fe I 6141 (187 mÅ), Fe I 6546 (167 mÅ), Fe I 6173 (105 mÅ), and Fe I 6157 (87 mÅ). The value in mapping several lines and then averaging the maps is that those features which are spurious for a single line will be supressed in the final average map. Note that the strong lines require a large, cool feature at the rotation pole which is not so obvious from the weaker lines. The effective surface resolution is ≈ 15° which is indicated by the surface grid size

5.3. Chromospheric electron densities

Model chromospheres of flare stars show the strength of the Hα emission to be very sensitive to the chromospheric electron density ($\propto n_e^3$; Cram & Mullan 1979). Given the adopted model assumptions, i.e., isothermal chromosphere optically thick at Hα, we may estimate chromospheric electron densities for the lower chromosphere of LQ Hya.

The chromospheric Doppler width of the line is given from

$$\Delta\lambda_D = \frac{\xi_D}{c}\lambda_0 = 12.85\left(\frac{T_{chrom}}{10^4 A}\right)^{\frac{1}{2}}\frac{\lambda_0}{c} \quad (2)$$

where A is the atomic weight of the atoms under consideration, λ_0 the rest wavelength, and ξ_D the velocity dispersion along the line of sight (Mihalas 1970). An isothermal chromosphere of temperature T_{chrom} = 10 000 K thus causes a Doppler width of $\Delta\lambda_D$ = 0.28 Å. According to the formulation of Cram & Mullan (1979) the optical depth is proportional to the ratio of the peak separation to the chromospheric Doppler width:

$$\ln \tau_{chrom} = \left(\frac{\Delta\lambda_{peak}}{2\Delta\lambda_D}\right)^2 \quad (3)$$

where $\Delta\lambda_{peak}$ is the separation between the "blue" and the "red" wavelength peaks. This quantity has been measured from the spectra and is listed in Table 3. The electron density is then given by

$$n_e = 1.67\,10^{14}\frac{F_{max}}{F_{cont}}\frac{B\,(T_{eff})}{B\,(T_{chrom})}\tau_{chrom}^{-1} \quad (4)$$

where F_{max}/F_{cont} is the ratio of the peak flux to the continuum flux and B is the Planck function. The former quantity is once again measured from our spectra and listed in Table 3 as a function of rotational phase. Using T_{eff} = 5100 K for a K2 dwarf and estimating T_{chrom} to be around 10 000 K, we find electron densities in the range of $1 - 5\,10^{11}$ cm^{-3}. The transition from collisional to photoionizational control of the line source function occurs at around $6\,10^{11}$ cm^{-3} for LQ Hya (see Cram & Mullan 1979, Eq. (8) – (11)). Thus our values are consistent with a "mixed"-type Hα line formation.

Table 3. Balmer-line measures

Phase	$\frac{F_{max}}{F_{cont}}$	FWHM (Å)	$\frac{F_{\Delta\lambda=0}}{F_{max}}$	$\frac{F_{red}}{F_{blue}}$	$\Delta\lambda_{peak}$ (Å)	$\log n_e$ (cm^{-3})
0.138	1.005	2.27	0.962	0.988	1.234	11.12
0.201	1.000	1.89	0.967	0.986	1.197	11.24
0.261	1.014	1.45	0.941	0.970	1.058	11.68
0.349	1.018	2.27	0.956	0.982	1.234	11.12
0.385	1.027	2.33	0.967	0.997	1.171	11.34
0.444	1.009	2.33	0.961	0.994	1.250	11.06
0.503	1.009	2.14	0.948	0.977	1.260	11.03
0.595	1.020	2.08	0.980	1.000	1.134	11.45
0.675	1.004	2.39	0.957	0.983	1.201	11.23

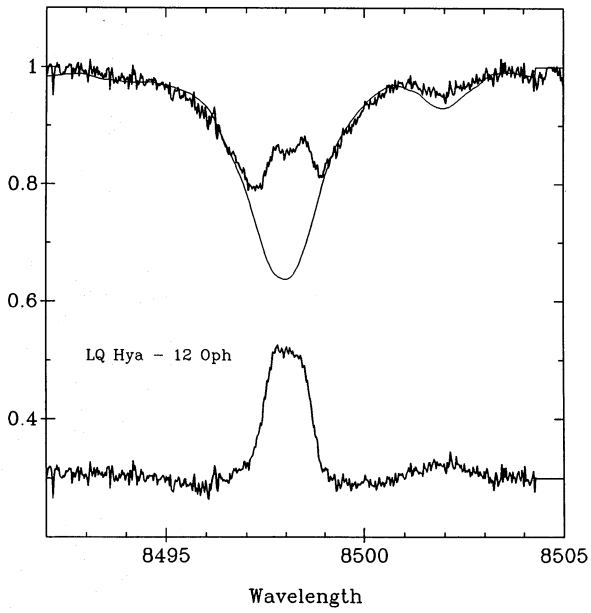

Fig. 7. Profile of the Ca II λ8498 Å line of LQ Hya at phase 0.533. A broadened spectrum of the K2V star 12 Oph is superimposed on the top spectrum (thin line) and subtracted from LQ Hya in the lower spectrum. Note the central reversal and the asymmetry of the "blue" and "red" core-emission peaks

5.4. Plages, prominences, or local velocity fields ?

Figure 9 shows the Hα line behavior as a function of rotational phase. The drop in full width at half maximum (FWHM) and peak separation $\Delta\lambda_{peak}$, and the variation of the line asymmetry F_{red}/F_{blue} at phase 0.2-0.3 coincide well with the variations of various photospheric line-depth ratios, continuum ratio V/I, and the light-curve *maximum* in Fig. 2b. A second drop at phase $\approx 0.5-0.6$, although not as convincing, coincides with a second light-curve "maximum" (actually an asymmetry in the decline better seen in $V - I$). Both phases concide with the passage of *unspotted* photospheric regions across the central meridian.

If the observed variations of the Hα-peak separation $\Delta\lambda_{peak}$ of $\approx$ 0.2 Å or 7 pixels are indeed real and not some sort of gross artifact, then the chromospheric optical depth at Hα line center changes from roughly 160 to 30 between rotational phase 0.503 and 0.595, i.e. within $\approx 30°$ on the stellar surface. A similar behavior is seen around phase 0.15-0.25. The measured FWHM seems to vary in the same sense, i.e. large widths at large peak separations and vice versa. The emission-peak asymmetry, expressed as F_{red}/F_{blue}, varies accordingly, as does the central reversal depth expressed in units of maximum peak intensity ($F_{\Delta\lambda=0}/F_{max}$). Radial velocity measurements of the Hα-line peaks relative to photospheric lines show no stochastic or systematic differences, thus entirely consistent with the Hα forming layers being relatively close to the stellar surface. Co-rotating prominences extending up to several stellar radii and passing in front of the stellar disk would significantly absorb the background chromospheric light and move through the Hα profile rather rapidly (cf. Collier-Cameron & Robinson 1989). We do

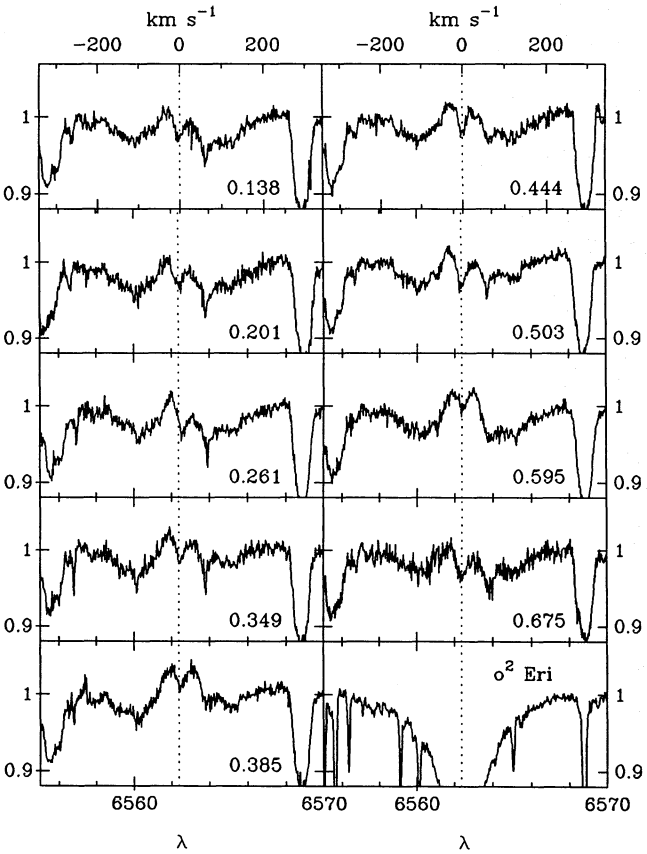

Fig. 8. Hα spectra of LQ Hya taken over slightly more than one half of a rotation cycle (P = 1.6 days). All spectra were obtained within two stellar rotations. Note that the asymmetry of the "red" to "blue" emission peaks changes with rotational phase but never really reverses its asymmetry. Maximum asymmetry occurs around phase "0.261" and gradually change to approximately equal peaks at phase "0.385". The line wings remain roughly constant and are reminiscent of an early K dwarf star (compare with the K1V standard o^2 Eri in the lower right panel)

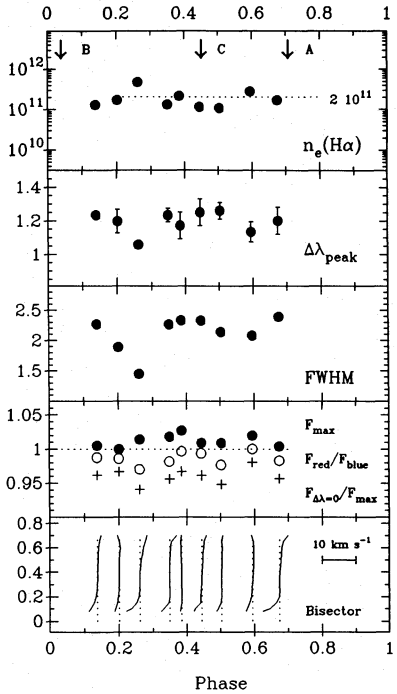

Fig. 9. Balmer Hα line behavior as a function of rotational phase. The longitudinal positions of spotted regions A, B, and C, are marked. From top to bottom is shown, the computed electron density n_e in cm^{-3} (mean value is indicated), the separation between blue and red emission peak $\Delta\lambda_{peak}$ in Å, the full width at half maximum (FWHM) of the central emission in Å, the maximum intensity F_{max}, the asymmetry between the red and the blue emission peak F_{red}/F_{blue}, the relative intensity of the core of the central reversal and, in the lower panel, the line bisectors of the excess emission-line profiles

not see transient absorption components nor any radial velocity variations and thus believe that prominences are unlikely to be the cause of the Hα variations. However, we caution that the time resolution of our observations would be too small to resolve these transient features. Plages in the lower chromosphere are probably a more likely explanation. Changes in the radial structure of the chromospheric heating function above photospheric spots might be another contributing source (Turner et al. 1991). Whether the observed variations are rotationally modulated or just time dependent cannot be said because of limited phase coverage of our observations. We would need at least two consecutive rotation cycles to distinguish between recurrent phenomena like plages or transient phenomena like (micro) flares (cf. Neff et al. 1989).

5.5. Are local chromospheric velocity fields spatially related to photospheric spots?

In this section, we will investigate whether the Hα line variations could also be explained by local chromospheric velocity fields. Crivellari et al. (1987) demonstrated the use of Ca II H spectra as a velocity field diagnostic for late-type dwarfs. We will attempt here to use Hα instead. Although the physical process of formation of these two lines is different they contain similar information. We subtracted a very high S/N spectrum of the K1V standard o^2 Eri from all individual LQ Hya scans to examine the excess emission profiles. The standard star spectrum was shifted and broadened to match the photospheric absorption lines of LQ Hya. The resulting excess emission lines may then represent the net chromospheric Hα emission. The profile shapes are rather well determined due to the high quality spectra and good sampling (50 pixels for the central 1.5 Å). The measured excess equivalent widths for LQ Hya depend, of course, upon the line profile of the adopted standard star and, since o^2 Eri is slightly earlier in spectral type than LQ Hya we cite here only a mean value taken over all phases: 1.04±0.02 Å (s.d.).

As a next step we computed bisectors for these excess emission lines. A particularly useful diagnostic for velocity fields is the velocity span between a point high up on the line bisec-

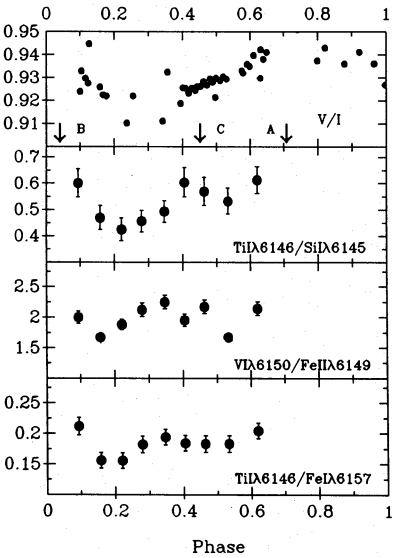

Fig. 10. Photospheric line-ratio variations. The longitudinal positions of spotted regions A, B, and C, are marked. From top to bottom is shown, the broad-band continuum ratio V/I from simultaneous photometry, the line-depth ratios for Ti I/Si I (χ = 1.87/5.61 eV), V I/Fe II (χ = 0.30/3.89 eV), and Ti I/Fe I (χ = 1.87/4.07 eV), respectively

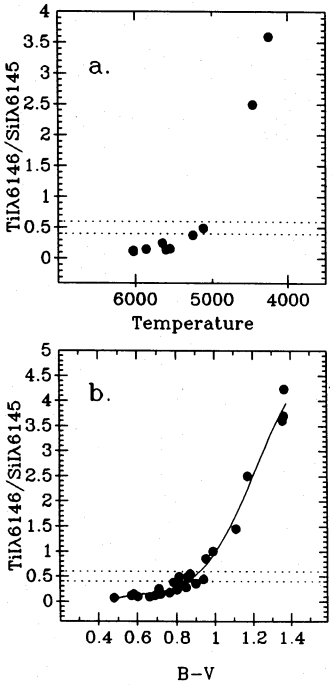

Fig. 11. Line-depth ratios Ti I 6146/Si I 6145 of selected standard stars versus effective surface temperature (panel *a*), and versus $B-V$ (panel *b*). The upper panel contains only $T_{\rm eff}$ standard stars from Bell & Gustafsson (1989), while the lower panel contains our 28 Morgan-Keenan class V standards. The dotted lines indicate the observed range for LQ Hya, and the full line in the lower panel is a polynomial fit to the data

tor (close to the line core in our case) and one near the bottom (residual intensity of 0.1 in our case). A *global* chromospheric velocity field would bend *all* bisectors in one direction which depends upon whether there is upwards or downwards flow. A *local* velocity field would modulate the bisectors such that they show a transition from "left" bent to "right" bent at a time of central meridian passage (see, e.g. Gray 1988; Toner & Gray 1988). The measured bisectors for LQ Hya are shown as a function of rotational phase in the bottom panel of Fig. 9. There is no immediately obvious change of the shape of the bisectors which would allow us a firm conclusion but we point out that the largest velocity spans occur at phase 0.26 and 0.67 and are on the order of 6.0±0.5 km s^{-1} as compared to 0.5±0.5 km s^{-1} at phases 0.385 and 0.503, respectively. Transitions from left-bent to right-bent might have occured around phases 0.22 and 0.62, prior to the most dominant $\mathscr{S}$ -shaped bisectors at times when the bright areas between the spots were crossing the central meridian (compare with Fig. 2b and note that stellar longitude is counted in the opposite direction than rotational phase with the zero-point at phase 0.75). The lower end of the bisectors in Fig. 9 are all bent toward the "blue" side and might indicate a presumably global, upward pointed flow pattern but is not well determined due to possible mismatches in the line wings of the synthezised spectra. We note that our standard stars o^2 Eri and 12 Oph do not show a similar bend. As pointed out by the referee, bright plages near the receding limb at phases $\approx$0.26 and 0.67 could also explain the time dependent variations of the upper bisector. Although possible, this explanation would be inconsistent with the fact that the FWHM at phase 0.26 shows a minimum while the velocity span of the bisector has a maximum. Because if we represent the plage contribution by a Gaussian emission component located at $\approx +v \sin i$ we should see a broader Hα line and thus a maximum in FWHM. Exactly the opposite is seen (Fig. 9). Moreover, the simultaneous $U-B$ color variations are in phase with the V-light curve and can be fully explained by cool photospheric starspots. Any plage contribution to the $U-B$ color is not directly obvious (Fig. 2b). Unfortunately, our observations cannot fully exclude a plage contribution (due to insufficient time resolution). Nor show the differential spectra with respect to o^2 Eri any conclusive sign of transient excess emission components, so we tend to believe that we see the combined effect of an asymmetric plage distribution and local velocity fields as the most likely cause for the observed Hα line variability. We conclude that, if plages and local chromospheric velocity fields are detectable on LQ Hya, they coincide with regions *between* photospheric spots (or possibly around the edges) reminiscent of the observed mass outflow around sunspots but that the observational evidence is only marginal.

6. Spot temperature from photospheric line-depth ratios

6.1. The "undisturbed" photospheric temperature

The first step was to re-examine the spectral type of LQ Hya from several line ratios to see if they are consistent with the previ-

ously assigned K2V classification. This was done by measuring ratios of line-depths of a series of temperature and/or luminosity sensitive lines and comparing these results with Morgan-Keenan standard stars. Four particularly useful line ratios were compared with data of standard stars taken from Strassmeier & Fekel (1990). They show that the various line ratios of LQ Hya are consistent with it being a K2±0.5 dwarf star. This is also in excellent agreement with the measured $B-V$ color. Bell & Gustafsson (1989) obtain a mean temperature of $\approx$ 5100 K for a K2V star from synthetic infrared colors as well as infrared flux ratios and we again adopt this value for the effective surface temperature of LQ Hya.

6.2. Spot temperature from line-ratio variations

Since some metallic lines have pronounced sensitivity to temperature and others not, observations of pairs of lines in which one is temperature sensitive and the other insensitive would allow a precise determination of the relative stellar surface temperatures. Problems with this technique are non-LTE effects in excitation, differential chemical abundances, and nonlinearities in the increase/decrease of the line strengths of different species with temperature. When comparing the temperatures of two stars, such effects can be expected to reduce the precision of the result, which Gray & Johanson (1991) give as ±10 K. However, if we observe a single star with an asymmetric surface temperature distribution and monitor it throughout its rotation cycle, differential abundance effects are not expected and we may use line ratios to obtain *mean* temperature differences. Here the mean temperature refers to the average over the visible stellar surface. Note that line ratios are not as affected by continuum displacements as are, e.g., equivalent widths.

We observed variations of line-depth ratios for several pairs of lines from the 6160 Å region spectra of LQ Hya (Fig. 10). These line-ratio variations are in phase with the continuum-ratio variations from V and I-band photometry (upper panel in Fig. 10) and are most pronounced for the line ratio Ti I 6146/Si I 6145 Å ($\Delta\chi_{\rm lines} \approx 3.7$ eV). This line pair has the highest change of ratio for a given temperature change, and we used it to obtain another value for the spot temperature totally independent from the temperature based on photometric variations (Sect. 3.3).

We measured spectra of 28 dwarfs in a 80 Å band centered at 6160 Å and used them to calibrate the Ti I/Si I ratio variations of LQ Hya (Fig. 11a,b). A polynomial fit through the data then defines an empirical relationship between $B-V$ color and line-depth ratio, given by

$$\frac{Ti}{Si} = 0.000586 - 8.17\,(B-V) + 44.09\,(B-V)^2 - 84.49\,(B-V)^3 + 68.69\,(B-V)^4 - 19.14\,(B-V)^5 \quad (5)$$

The $B-V$ indices were converted to effective temperature using standard transformations (cf. Gray 1988). No fit was obtained for the data in Fig. 11a due to the limited number of stars observed, but visual inspection shows the line-ratio variations with $T_{\rm eff}$ to be consistent with the polynomial fit from $B-V$. With the calibration in Eq. (5), the observed range of 0.20±0.04 (0.42 - 0.62) of the line-ratio variations of LQ Hya translates into a surface-temperature variation of 180±20 K, that is 4910 through 5090 K in absolute temperature. The error in the relative temperature was estimated by repeated measurements of the spectra and by determining the effect of an 0.5 % displacement of the continuum. Note that the temperature from the lower bound of the observed line-depth ratio (5090 K) is consistent with the 5100 K temperature for a K2V star given by Bell & Gustafsson. The variation of the mean temperature of 180 K agrees with the value computed from the spot temperature and area given in Table 2.

7. Summary and conclusions

In this paper we present a photometric and spectroscopic study of inhomogeneities in the photosphere and the lower chromosphere of the young, rapidly rotating K2 dwarf LQ Hya. We applied the Doppler imaging technique to nine absorption lines of various strengths, excitation potentials, and $\log gf$ values, and produced a *combined* map from all individual maps. By averaging all the maps together spurious features from a single line will be suppressed in the final map. This procedure greatly enhances the reliability of the reconstructed surface image. However, there seems to be a systematic change in the appearance of the map near the pole with the equivalent width of the line used for the mapping. Although the polar feature decreases with decreasing equivalent width, a very high latitude part persists in all maps. We used three different indicators to derive the maximum difference in surface temperature between spotted and unspotted regions. The three methods, color variations, line-depth ratio variations, and Doppler imaging, gave consistent results of 500 K. Extended regions of lesser temperature depression are also evident. Simultaneous observations of the Hα line profile suggest that lower electron densities occur at times when a cool starspot is in view, indicating a less dense chromosphere above spotted regions. At phases when the least-spotted regions crossed the central meridian, the FWHM of the Hα emission showed a minimum and the line bisectors a transition from "left" bent to "right" bent. Unfortunately, the significance of the observed line profile variability is only marginal and does not allow a conclusive decision whether plages or local chromospheric velocity fields cause the variations. Nevertheless we tentatively conclude that if local velocity fields and plages exist on LQ Hya, they coincide with regions between photospheric spots or possibly around their edges. This could be reminiscent of the observed mass outflow around sunspots.

Acknowledgements. We are grateful to the referee, Dr. Bernard Foing, for his helpful suggestions which led to an improvement of this paper. KGS wishes to acknowledge support from the Austrian Fond zur Förderung der wissenschaftlichen Forschung (FWF) under grant P7993. JBR and WHW acknowledge support from the Natural Sciences and Engineering Research Council of Canada (NSERC). JMM is grateful for support from an NSERC operating grant to A.F.J. Moffat.

References

Al-Naimiy, H., 1978, Ap&SS 53, 181
Ambruster, C., Fekel, F. C., 1990, BAAS 22, 857
Andersen, J. 1991, A&AR 3, 91
Bell, R. A., Gustafsson, B., 1989, MNRAS 236, 653
Bidelman, W. P., 1981, AJ 86, 553
Collier-Cameron, A., Robinson, R. D., 1989, MNRAS 236, 57
Cram, L. E., Mullan, D. J., 1979, ApJ 234, 579
Crivellari, L., Beckman, J. E., Foing, B. H., Vladilo, G., 1987, A&A 174, 127
Cutispoto, G., 1991, A&AS 89, 435
Dempsey, R. C., Bopp, B. W., Henry, G. W., Hall, D. S., 1992, ApJS, in press
Donati, J.-F., Brown, S. F., Semel, M., et al. 1992, A&A, in press
Eggen, O. C., 1984, AJ 89, 1358
Fekel, F. C., Bopp, B. W., Africano, J. L., Goodrich, B. D., Palmer, L. H., Quigley, R., Simon, T., 1986a, AJ 92, 1150
Fekel, F. C., Moffett, T. J., Henry, G. W., 1986b, ApJS 60, 551
Gray, D. F., 1988, in: Lectures in Spectral Line Analysis: F, G, and K stars, The Publisher, Western Ontario.
Gray, D. F., Johanson, H. L., 1991, PASP 103, 439
Hall, D. S., 1991, in: Tuominen I., Moss D., and Rüdiger G. (eds.), Proc. of IAU Colloq. 130, The Sun and Cool Stars: activity, magnetism, dynamos, Springer-Verlag, Berlin-Heidelberg-New York, p. 353
Jetsu, L., 1990, in: Muionen K., et al. (eds.), Proc. Finnish Astr. Soc., p. 5
Kürster, M., Hatzes, A. P., Pallavicini, R., Randich, S., 1992, in: Giampapa, M. (ed.), Proc. of the 7th Cambridge Workshop, Cool Stars, Stellar Systems, and the Sun, PASPC, in press
Kurucz R., 1979, ApJS 40, 1
Linsky, J. L., Hunten, D. M., Sowell, R., Glackin, D. L., Kelch, W. L., 1979, ApJS 41, 481
Mihalas, D., 1970, Stellar Atmospheres, San Fransisco, Freeman, p. 250
Neff, J. E., Walter, F. M., Rodonó, M., Linsky, J. L., 1989, A&A 215, 79
Pasquini, L., Cutispoto, G., Gratton, R., Mayor, M., 1991, A&A 248, 72
Pettersen, B. R., 1989, A&A 209, 279
Piskunov, N. E., Rice, J. B., 1992, Crimean Journal of Astrophy., in press
Piskunov, N. E., Tuominen, I., Vilhu, O., 1990, A&A 230, 363
Rice, J. B., Wehlau, W. H., Khokhlova, V. L., 1989, A&A 208, 179
Saar, S. H., Neff, J. E., 1991, in: Wallerstein, G. (ed.), Proc. of the 6th Cambridge Workshop, Cool Stars, Stellar Systems, and the Sun, PASPC 9, 171
Saar, S. H., Piskunov, N. E., Tuominen, I., 1992, in: Giampapa, M. (ed.), Proc. of the 7th Cambridge Workshop on, Cool Stars, Stellar Systems, and the Sun, PASPC, in press
Schmidt-Kaler, T., 1982, in: Schaifers K. and Voigt, H. H. (eds.), Landolt-Börnstein, Vol. 2b, Springer-Verlag, Berlin-Heidelberg-New York, p. 1
Shine, R. A., Linsky, J. L., 1972, SP 25, 357
Simon, T., 1990, ApJ 359, L51
Strassmeier, K. G., 1988, Ap&SS 140, 223
Strassmeier, K. G., Bopp, B. W., 1992, A&A 259, 183
Strassmeier, K. G., Fekel, F. C., 1990, A&A 230, 389
Strassmeier, K. G., Fekel, F. C., Bopp, B. W., Dempsey, R. C., Henry, G. W., 1990, ApJS 72, 191
Strassmeier, K. G., Hall, D. S., 1988, ApJS 67, 453
Strassmeier, K. G., Rice, J. B., Wehlau, W. H., et al., 1991, A&A 247, 130
Toner, C. G., Gray, D. F., 1988, ApJ 334, 1008
Turner, N. J., Cram, L. E., Robinson, R. D., 1991, MNRAS 253, 575
van Leeuwen, F., Alphenaar, P., 1982, ESO Messenger 28, 15
Vilhu, O., Gustafsson, B., Walter, F. M., 1991, A&A 241, 167
Vogt, S. S., 1988, in: Cayrel de Strobel, G., Spite, M. (eds.), Proc. IAU Symp. 132, The Impact of very high S/N Spectroscopy on Stellar Physics, Kluwer Dordrecht, p. 253
Vogt, S. S., Hatzes, A. P., 1991, in: Tuominen, I., Moss, D., Rüdiger, G. (eds.), Proc. IAU Colloq. 130, The Sun and Cool Stars: activity, magnetism, dynamos, Springer-Verlag, Berlin-Heidelberg-New York, p. 297

This article was processed by the author using Springer-Verlag LaTeX A&A style file version 3.